

Computer Simulation of Controlled Radical Polymerization: Effect of Chain Confinement Due to Initiator Grafting Density and Solvent Quality in “Grafting From” Method

Salomon Turgman-Cohen and Jan Genzer*

Department of Chemical and Biomolecular Engineering, North Carolina State University, Raleigh,
North Carolina 27695-7905, United States

Received September 3, 2010; Revised Manuscript Received October 11, 2010

ABSTRACT: We use stochastic Monte Carlo simulation following the bond fluctuation model to study the effects of grafting density of surface-anchored initiators and solvent quality on controlled radical polymerization (CRP) from flat impenetrable substrates under good and poor solvent conditions. Our CRP model includes a mechanism for activation/deactivation of the chains and neglects termination and chain transfer reactions. The system is, thus, “truly living”. We find that under these conditions, surface-initiated polymerizations at low grafting densities resemble those in the bulk. In contrast, at high initiator grafting densities, these surface-initiated polymerizations result in gradients of the free monomer and chain-end concentrations, which lead to an uneven growth of the chains and ultimately yield polymers with broad molecular weight distributions. Poor solvent conditions exacerbate this problem by collapsing the chains and in some cases forming chain aggregates, which further restrict the access of free monomers by the active polymer chain ends and contribute to their uneven growth and ultimately broader length distributions relative to good solvent conditions. While at low grafting densities the molecular weight distributions can be described by the conventional Schulz-Zimm distribution function, at high grafting densities this approach fails to describe accurately the dispersity in chain lengths.

Introduction

During the past decade, numerous research reports have demonstrated that specialty end-tethered polymer layers on surfaces can be generated by “grafting from” polymerization using controlled radical polymerization (CRP) schemes.^{1–10} Equilibrium between active polymerizing chains and inactive dormant chains in CRPs is shifted heavily towards the dormant chains, which leads to controlled molecular weights and molecular weight distributions (MWDs).^{11,12} The “grafting from” scheme consists of growing polymers directly from initiator-covered surfaces. In contrast to the “grafting onto” approach, in which polymers with reactive end groups attach to the surface, the “grafting from” strategy is believed to yield dense brushes with controlled thickness, grafting densities, and relatively narrow MWDs characterized by a small polydispersity index (PDI). Despite the common use of CRP for the synthesis of end-tethered layers, there is a dearth of research characterizing the PDI of polymers produced from initiating surfaces. The current approach for the estimation of PDI in tethered layers involves the addition of free bulk initiators to the polymerization mixture and the subsequent analysis of the solution-synthesized polymers by size-exclusion chromatography (SEC) or an equivalent technique. The major drawback of this approach is that it neglects possible effects of surface confinement and diffusion of the reactive components to and from the propagating radical ends, which, in turn, affect the ability of CRP to yield grafted polymers with low PDI.

Surface-initiated atom transfer radical polymerization (SI-ATRP) and its various derivatives (i.e., ARGET ATRP) are probably the most frequently used CRP schemes employed in the formation

of polymeric grafts on surfaces using the “grafting from” method.^{13,14} The popularity of these methodologies has stemmed from their robustness, insensitivity to the presence of small amounts of impurities (most notable oxygen) that tend to terminate the radical processes, and their ability to create copolymers and polymers with complex topologies. In spite of a sizable amount of work on this topic, our understanding of the “grafting from” process and complete characterization of the properties of grown macromolecular grafts has been hindered by many technical limitations. As a result, contradicting reports have not been reconciled conclusively by means of our current knowledge.^{15–19} For example, experimental studies performed by cleaving the surface-initiated polymers^{15–19} report both increases^{15,16,18} and similar¹⁷ PDIs of the surface-grafted polymers relative to polymers grown in the solution. In addition, while most reports noted that “grafting from” polymerization resulted in polymers whose molecular weights were lower than polymers grown under identical experimental conditions in the bulk, Koylu et al. reported recently on the opposite trend.¹⁸ These and other findings are not easy to understand without performing a comprehensive set of additional experiments involving SEC measurements with very sensitive concentration detectors. However, even with the available SEC measurements of surface-grown polymers, more information about the structure of the grafted layer is needed in order to comprehend the effect of the various process parameters that influence the “grafting from” mechanism. In spite of tremendous progress in various instrumentation tools, no currently available analytical technique is capable of characterizing completely the structure of the grafted layer. Computer simulations and various molecular theories may prove useful because they provide monomer-level insight into the polymerization process that may not be accessible to

*To whom correspondence should be addressed. Tel.: +1-919-515-2069. E-mail: jan_genzer@ncsu.edu.

experiments. These approaches further offer the opportunity to vary systematically the parameters of the polymerization system and to characterize completely the properties of the molecular grafts without the limitations involved with experiments.

The variations in PDI investigated herein are relevant given that properties such as the brush height and the polymer concentration profile vary significantly when comparing grafted polymers with equal number average molecular weights ($\langle N \rangle$) but differing MWDs.^{20–29} For instance, using numerical self-consistent mean field theory de Vos and Leermakers²⁹ demonstrated recently that broadening of MWDs leads to changes of the shapes of the brush concentration profiles from parabolic to linear to concave and to corresponding increases in the brush layer thickness under good solvent conditions. The authors also noted that, interestingly, the scaling exponents for the brush height with respect to the molecular weight and the grafting density are identical for both monodisperse and polydisperse polymers. In a later study, the authors reported on the effect of PDI on the antifouling properties of tethered polymers, which is an important application of these layers.³⁰ In this contribution, we build upon previous reports and investigate the effect of the initiator grafting density and the solvent quality on the properties of polymers initiated from flat substrates; and how they compare to bulk initiated reactions in athermal solvents. The results provide information about the molecular weight, PDI, and concentration profiles for grafted polymers grown by CRP reactions.

Reports simulating and modeling surface-initiated polymerization have appeared previously. Wittmer et al.³¹ studied the diffusive growth of a polymer layer by *in situ* polymerization using a mean-field treatment and scaling theories of polymers in good solvents. Computer simulations utilizing the bond-fluctuation model (BFM) were used to verify the developed theory. Wittmer and co-workers considered a system in which initiators, which could commence irreversible growth of linear unbranched chains, covered densely an impenetrable wall. The authors further assumed that the chain growth was slow and, therefore, the chains retained their local equilibrium conformation during the polymerization process. An infinitesimal flux of incoming monomers then provided the reactants from which the polymers could grow. Wittmer et al. predicted that for diffusion-limited reactive growth the formed chains would be polydisperse but nonetheless strongly stretched away from the surface.

Numerous computer simulation studies have been performed on bulk- and surface-initiated equilibrium, “living” polymerizations, in which polymerization and depolymerization reactions were accounted for and the polymers were in chemical equilibrium with a population of free monomers. Using off-lattice and BFM Monte Carlo (MC) simulations, Milchev and co-workers³² reported briefly on the effect of growing polymers from low and high initiator grafting densities that resulted in differences in their MWDs. Matyjaszewski et al.¹³ also implemented computer simulations to investigate surface-initiated polymerizations. They constructed concentration profiles and computed the MWD of the simulation-grown polymers.

Recently, Liu and co-workers³³ reported on the effects of the polymerization rate and the density of initiating centers on the properties of macromolecules grown by “grafting from” polymerization from flat substrates by means of coarse-grained molecular dynamics. Liu et al. modeled a “true” living/controlled polymerization process by not considering any termination (or chain transfer) in their simulations. They demonstrated that decreasing the rate of polymerization resulted in polymeric grafts with lower PDI, relative to polymerization performed at higher rates. Liu et al. also reported on the interplay between the density of the initiators on the surface, their effectiveness of initiation, and polymerization rates. Specifically, the authors pointed out that in systems with low initiator density nearly all initiators

started polymerization. At slow polymerization rates, all chains propagated at approximately the same rate. In contrast, at high densities of the initiator centers, initiation efficiency decreased with increasing rate of polymerization, which, in turn, resulted in a higher fraction of inactive initiators and higher PDIs.

A few years ago, one of us developed and presented a computer simulation model of controlled radical polymerization resembling processes occurring in ATRP by employing a stochastic MC scheme.³⁴ We described how $\langle N \rangle$ and the MWD of polymers grown in bulk and on flat impenetrable surfaces depended on a number of parameters, such as, the concentrations of different species and the simulation equivalents to kinetic rates and equilibrium constants. We demonstrated that increasing the termination probability and decreasing the initial probability of addition of a new monomer to a growing chain broadened the MWD. Our results also indicated that confinement of surface-initiated polymers resulted in increased numbers of early terminations, which, in turn, led to higher PDIs. Upon increasing the grafting density of the initiators on the surface, we noted further increases in the PDIs of the grafted polymers.

The current work builds upon our previous MC study³⁴ and the work of Liu and co-workers³³ to investigate the effect that decreasing the solvent quality and/or grafting the initiators to the surface has on the broadness of the MWDs. By turning off the termination reaction and decreasing the rate of polymerization (in contrast to our previous work), we aim to model the “true living”/controlled radical process. In contrast to previous studies, we include a mechanism for activation/deactivation of the propagating species that resembles most CRP schemes in our simulations. We will demonstrate that even in “truly living” polymerizations, confining the growing chains (either by grafting to the surface or by collapsing the chains in poor solvents) may result in appreciable increases in the PDI of the surface-tethered polymers. We also explore the effect of confinement due to chain collapse on the MWDs. Our motivation for investigating polymerization in poor solvents comes from experimental studies in which methanol/water/monomer mixtures were used for SI-ATRP of methyl methacrylate (MMA)^{19,35} and *n*-isopropylacrylamide (NIPAAm)^{36–40} from planar substrates. If large monomer concentration gradients develop in these reactions, they can expose the grafted polymers to a water/methanol mixture, which is a poor solvent at the experimental conditions.

Simulation Model

Computer simulations of CRP reactions are performed by implementing a stochastic MC algorithm³⁴ in conjunction with the BFM.⁴¹ The polymers and monomers reside in a three-dimensional cubic lattice in which the monomers can be bonded according to the following vector families: P(2,0,0), P(2,1,0), P(2,1,1), P(2,2,1), P(3,0,0), and P(3,1,0).⁴² These vector sets prevent any bonds from crossing and monomers (and polymers) from overlapping as long as the only allowed moves in the simulation are nearest neighbor ones. The fluctuating character of the bond-lengths in this model allows for close approximation of continuum behavior while at the same time preserving the advantages of lattice models such as integer arithmetic.

The BFM is, by its nature, self-avoiding and as such it describes polymer behavior under good solvent conditions. To simulate poor solvent conditions we have incorporated a set of intermolecular, intramolecular and bond-length potentials.⁴³ The first potential is of the Lennard-Jones (LJ) form and is truncated to only act between beads that find themselves within the maximum distance allowed by the above-mentioned vector families (bond length = $10^{1/2}$). A bond-length potential is also included to describe the increase in chain stiffness with decreasing temperature. In our system, the LJ and bond-length potentials only act

Table 1. Lattice Dimensions and the Corresponding Values of σ

$L_x = L_y$	L_z	lattice Volume	σ
160	39	998400	0.06
140	51	999600	0.08
120	69	993600	0.11
100	100	1000000	0.16
80	156	998400	0.25
60	278	1000800	0.44

between bonded beads in the simulation box and not between the beads representing free monomers. We neglect the polymer–monomer and monomer–monomer interactions to prevent aggregation of free monomers that would describe an unlikely physical condition in which the monomers are not soluble in the polymerization medium. It was demonstrated previously that increasing the interaction parameter (ϵ) in these potentials relative to temperature led to collapsed chain conformations.^{43,44} We confirm independently chain collapse in the bulk- and surface-initiated cases (see Supporting Information) and perform reactive simulations in both good ($\epsilon = 4 \times 10^{-7} k_B T$) and poor ($\epsilon = 4 \times 10^{-1} k_B T$) solvents.

The MC algorithm used to simulate the polymerization reactions has been described previously.³⁴ The total number of initiators and monomers is fixed for all simulations performed. We vary the density of initiators on the surface while maintaining nearly constant the overall volume of the lattice by adjusting the dimensions of the cubic lattice ($L_x = L_y, L_z$). In this manner, we can investigate the effect of the grafting density of initiators on the polymerization while keeping other relevant parameters (i.e., monomer concentration) unchanged. Table 1 tabulates the $L_x = L_y$ and the L_z dimensions of the lattices used in this study and the resulting surface density of the initiators (σ , where $\sigma = 1$ represents a fully covered surface in the BFM). In bulk-initiated polymerizations, we implement periodic boundary conditions in the three spatial directions. For surface-initiated polymerizations, two impenetrable walls are located at $z = 0$ and $z = L_z$ representing the substrate and the limit of the simulation box, respectively; the periodic boundary conditions are employed only in the xy plane of the lattice.

The initial configuration for bulk-initiated polymerizations corresponds to the monomers and initiators distributed uniformly throughout the volume of the simulation box. Each initiator corresponds to two bonded polymer beads, of which one is a propagating center (i.e., chain end). In the case of surface-initiated polymerizations, the inactive bead of the initiator is located at equally spaced intervals on the substrate and at $z = 1$, while the propagating bead is placed directly above of the anchoring bead at $z = 3$. In the surface-initiated case, the bead adjacent directly to the surface is not movable. The numbers of monomers and initiators have been fixed at $M_o = 12500$ and $I_o = 400$, respectively; this corresponds to a lattice occupancy of 10.64%. We perform a preliminary long equilibration run consisting of $\approx 10^9$ attempted Monte Carlo steps (MCS, defined as MC steps per simulation bead) to obtain a randomly distributed configuration. The equilibrated configuration serves as input to the MC simulations.

We initialize the simulations by a short equilibration period of 10^6 MCS. This is equivalent to every bead in the simulation box undergoing, on average, 75 attempted moves. Once the second pre-equilibration finishes the reactive MC algorithm commences. The reactive MC scheme continues until either 80% of the monomer is exhausted (i.e., polymerized) or a predetermined maximum number of MCS elapses. The latter premature end of the simulations before reaching high conversions was necessary because, in the high surface density and poor solvent regimes probed, the polymerization rate is very slow and the simulation would not reach 80% conversion in a reasonable time.

The MC algorithm implemented here is similar to our previous work³⁴ except for a few changes that we describe next. Previously, the probability of reaction versus motion was set a priori to $P_r = 0.5$. In the current work, we investigate the effect of this parameter on the results of the simulation and determine that, for the study of different levels of confinement and poor solvent conditions, a more appropriate value of P_r is 0.01 (see Supporting Information). Reducing the reaction rate (propagation only in the present work since we prohibit termination and chain transfer) further assures controlled polymerization growth, which is consistent with the approach of Liu and co-workers. Reducing P_r also shifts the system behavior from a diffusion-limited reaction to a kinetically limited one, in turn, mitigating the effects of gradients in the free monomer volume fraction and allowing the polymer chains to approach their equilibrium conformations. Although it would be desirable to slow the reaction rate enough to achieve full kinetic control, balancing this need with feasible simulation times was required. The second difference between the current simulations and our previous work is that the probability to add a monomer (P_a) is no longer proportional ($P_a = P_{a,o}[M/M_o]$, where $P_{a,o}$ is a constant and M is the instantaneous number of free monomers) to the number of free monomers left in the simulation box. This proportionality was redundant because the probability that an active chain and a free monomer approach to within the reactive distance is already proportional to the instantaneous monomer concentration. We therefore modify our approach in the current work and set $P_a = P_{a,o}$ throughout the simulation run. Both of these changes affect the observed results in an absolute fashion, but all the observed trends and conclusions of our previous work³⁴ remain unchanged in this revision of the algorithm.

During a typical polymerization run, we monitor the monomer conversion (x_m), polydispersity index (PDI), radius of gyration ($|R_g^{2,1/2}|$), volume fraction profiles ($\phi_i(z)$), and the number of nearest neighbor site per active chain-end occupied by monomers (θ_m), polymers (θ_p), and chain ends (θ_e). We evaluate the PDI, R_g , and $\phi_i(z)$ at steps of 1% monomer conversion. We average these quantities for at least three independent runs to gain statistical certainty. The number of the nearest neighbors to the active chain ends are computed every 10000 MCSs and plotted as a function of monomer conversion. These data are fitted with a third degree polynomial to discern the trends between the different runs.

Results and Discussion

Solvent Quality. Computer simulations of polymerization reactions were performed in good and poor solvents for bulk-initiated systems. The working hypothesis was that with decreasing the solvent quality, the coil becomes more compact thus making the interior of the coil inaccessible to monomers and hiding the growing chain inside the collapsed coil. As a result, relative to polymerization under good solvent conditions, the rate of polymerization under poor solvent conditions will be slower and the PDI will increase. Figure 1 depicts the evolution of the $|R_g^{2,1/2}|$ (a) and PDI (b) as a function of monomer conversion for polymerizations performed in good (blue squares) and poor (red circles) solvent conditions. Compared to polymers grown in good solvents, under poor solvent conditions the resulting macromolecules possess smaller dimensions for identical average molecular weights (or monomer conversions). Moreover, the PDI of polymers grown under poor solvent conditions increases at higher conversions relative to the good solvent case.

While these observations confirm that chain collapse under poor solvent conditions and the resulting confinement of the propagating centers lead to broader MWDs, to gain insight into the reasons for this broadening, we have to

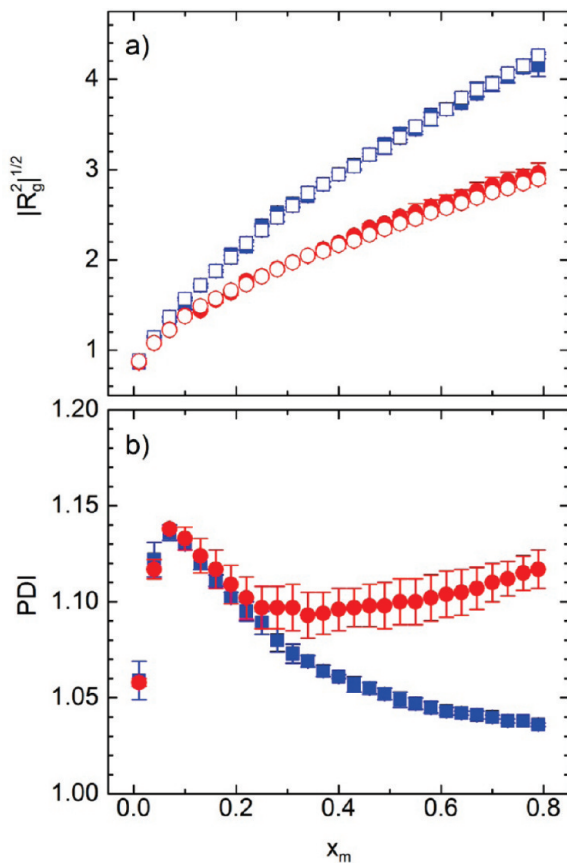


Figure 1. (a) Radius of gyration and (b) polydispersity index of bulk polymers in good (blue squares, $\varepsilon = 4 \times 10^{-7} k_B T$) and poor (red circles, $\varepsilon = 4 \times 10^{-1} k_B T$) solvent conditions as a function of monomer conversion.

monitor the environment around the propagating chain ends. Specifically, for every 10000 MCSSs we determine the number of nearest neighbor sites per active chain end occupied by monomers (θ_m), polymer beads belonging to the observed chain end ($\theta_{p,s}$) or to other chains ($\theta_{p,o}$), and the remaining empty sites (θ_e). We least-squares fit these data to facilitate the identification of differences between good and poor solvent conditions (Figure 2). In contrast to polymerization under good solvent conditions, in poor solvents there is a lower likelihood that an active chain-end will encounter a monomer and undergo reaction as reflected by the data for θ_m . Concurrently, $\theta_{p,s}$ and $\theta_{p,o}$ increase in going from good to poor solvent conditions. The increase in $\theta_{p,s}$ indicates that the chains are collapsing and that chain ends are more likely to neighbor other beads in the same chain. The increase in $\theta_{p,o}$ suggests that the chains tend to aggregate in poor solvent conditions, thus, further shielding the active chain ends and hindering the polymerization reaction. Both of these effects can disrupt monomer delivery to the chain ends, which can explain the decreased rate of polymerization (not shown) and the increase in PDI. One explanation for the increase in PDI that we cannot currently verify is that each chain might collapse with its chain end located farther or closer to the interphase between the collapsed globule and the solution. The dynamics of a collapsed chain are slow enough that the chain will not change its configuration significantly throughout the polymerization. This would result in uneven growth of chains depending on the specific collapse configuration.

While the aforementioned observations are specific to our model reaction, they provide insight into the factors

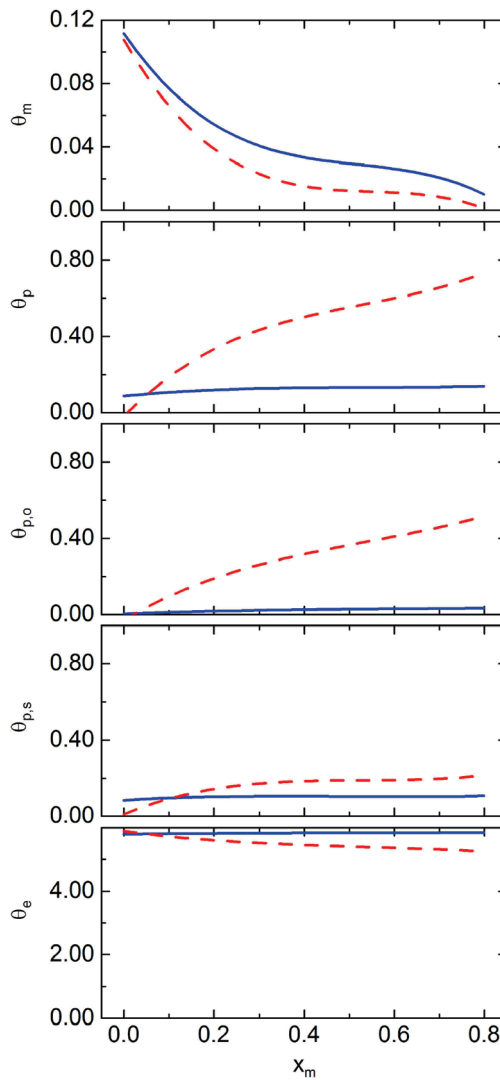


Figure 2. Average number of nearest neighbor sites per active end occupied by free monomers (θ_m), polymers (θ_p), polymers belonging to a different chain ($\theta_{p,o}$), polymer belonging to the observed chain ($\theta_{p,s}$), and the remaining empty sites (θ_e) for bulk polymerization under good (solid, $\varepsilon = 4 \times 10^{-7} k_B T$) and poor (dashed, $\varepsilon = 4 \times 10^{-1} k_B T$) solvent conditions.

influencing a real system. Take, for example, ATRP reactions, in which a terminal halogen atom can transfer reversibly to a neighboring metal/organic ligand complex protecting and deprotecting the chains.⁴⁵ In this case, not only will the collapse of the chain obstruct the monomer from reaching the reaction centers but it will also hinder the metal/organic ligand complex and the catalyst crucial for the reaction. One can therefore envision situations in which collapsed polymers do not alternate efficiently between the active (living) and inactive (dormant) forms resulting in deterioration of reaction control. Many other factors may come into play under poor solvent conditions (i.e., altered halogen transfer between the metal/ligand complex and the growing chain) and, in this sense, our simulations represent a simplified scenario providing insight into the factors affecting polymerization control in poor solvents.

Surface Density. Computer simulations of polymerizations were performed with bulk and surface-bound initiators under good and poor solvent conditions. Our benchmark system corresponds to a lattice defined by $L_x = L_y = L_z = 100$ with the initial number of monomers equal to 12500 and

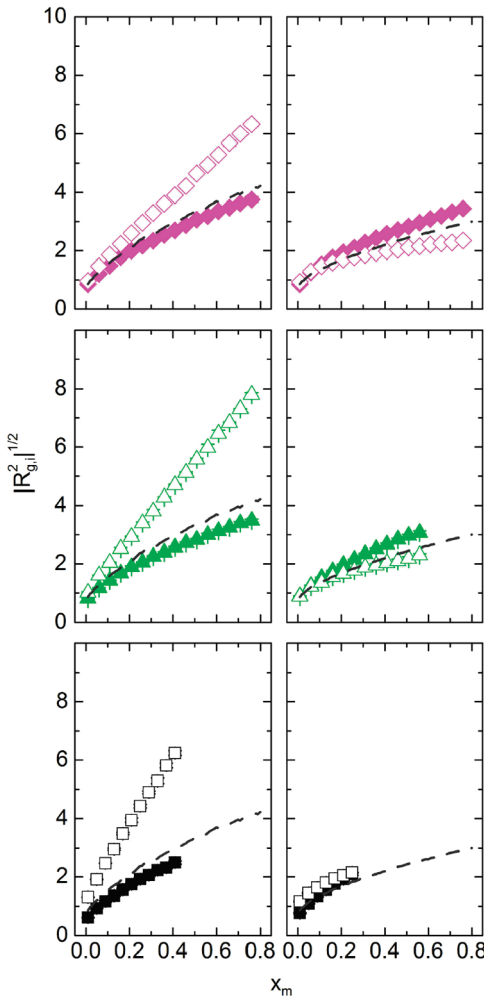


Figure 3. Parallel ($R_{g,\parallel}$, closed symbols) and perpendicular ($R_{g,\perp}$, open symbols) components of the average radius of gyration of grafted chains as a function of monomer conversion for good (left column, $\varepsilon = 4 \times 10^{-7} k_B T$) and poor (right column, $\varepsilon = 4 \times 10^{-1} k_B T$) solvent conditions at three different grafting densities (σ): 0.08 (top row, magenta), 0.16 (middle row, green), and 0.44 (bottom row, black). The dashed lines represent corresponding data for chains polymerized in bulk.

number of initiators equal to 400. In the surface-initiated polymerization, this corresponds to $\sigma = 0.16$. We also explore how varying σ affects the polymerization reaction. While a logical way to change σ would seem to be to add more initiators to the surface, this approach would alter the ratio between numbers of monomers and initiators, which would consequently influence the kinetics and PDI of the reaction. To achieve different values of σ without changing the numbers of monomers and initiators, one should thus modify the dimensions of the lattice to vary the area per initiator molecule while keeping the total volume of the lattice approximately constant. Given that L_z varies for simulations at different σ , all runs are inspected to ensure that the perpendicular component of the radius of gyration ($|R_{g,\perp}|^{1/2}$) does not approach L_z .

Figure 3 shows the parallel ($|R_{g,\parallel}|^{1/2}$) and perpendicular ($|R_{g,\perp}|^{1/2}$) components of the radius of gyration as a function of the monomer conversion for bulk- (dashed line) and surface-initiated (symbols) systems under good (left column) and poor (right column) solvent conditions at three different σ equal to 0.08 (top), 0.16 (middle), and 0.44 (bottom). We must note that the averages computed here are not ensemble

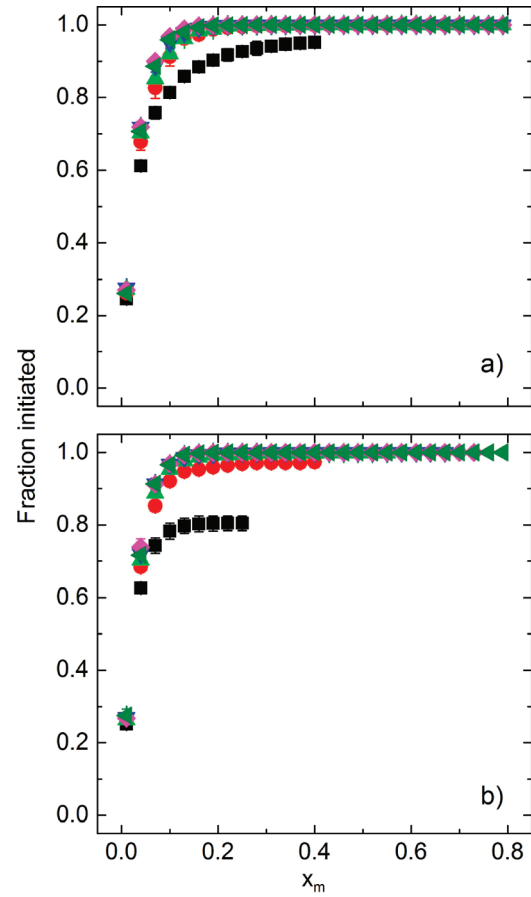


Figure 4. Initiator efficiency as a function of monomer conversion for a) good ($\varepsilon = 4 \times 10^{-7} k_B T$) and b) poor ($\varepsilon = 4 \times 10^{-1} k_B T$) solvent conditions at various grafting densities (σ): 0.06 (dark green left-pointing triangle), 0.08 (pink diamond), 0.11 (blue downward triangle), 0.16 (light green triangle), 0.25 (red circle), and 0.44 (black square).

averages for configurations of a single chain, but the averages of the instantaneous configurations of a population of chains with varying degrees of polymerization (N). Bulk polymers exhibit equal dimensions in every direction because of orientational averaging over many conformations and are therefore represented by a single line. The average size of the bulk-initiated polymers increases with increasing conversion; the increase is slower in poor solvents relative to good solvents, as noted previously. Surface-initiated polymers in good solvents exhibit larger dimensions in the direction perpendicular to the substrate than parallel to it; this effect becomes more pronounced with increases in σ . This shape asymmetry is due to repulsive excluded volume interactions between neighboring chains, which force the polymers to extend away from the tethering surface. Most of the shape asymmetry manifests itself as an increase in $|R_{g,\perp}|^{1/2}$, while the $|R_{g,\parallel}|^{1/2}$ undergoes only a small decrease from its bulk value. Under poor solvent conditions and at low σ $|R_{g,\perp}|^{1/2}$ becomes smaller than $|R_{g,\parallel}|^{1/2}$. With increasing σ , the difference between $|R_{g,\perp}|^{1/2}$ and $|R_{g,\parallel}|^{1/2}$ vanishes and eventually $|R_{g,\perp}|^{1/2} > |R_{g,\parallel}|^{1/2}$. These observations reveal that under poor solvent conditions the chains try to minimize their contact with the solvent. At low grafting densities, they achieve this by collapsing onto the substrate and stretching toward their neighbors. At higher grafting densities, the horizontal confinement increases and the only direction the chains can extend to is that perpendicular to the substrate.

In an ideal system, one would want all initiator molecules to activate simultaneously so that the propagation reaction

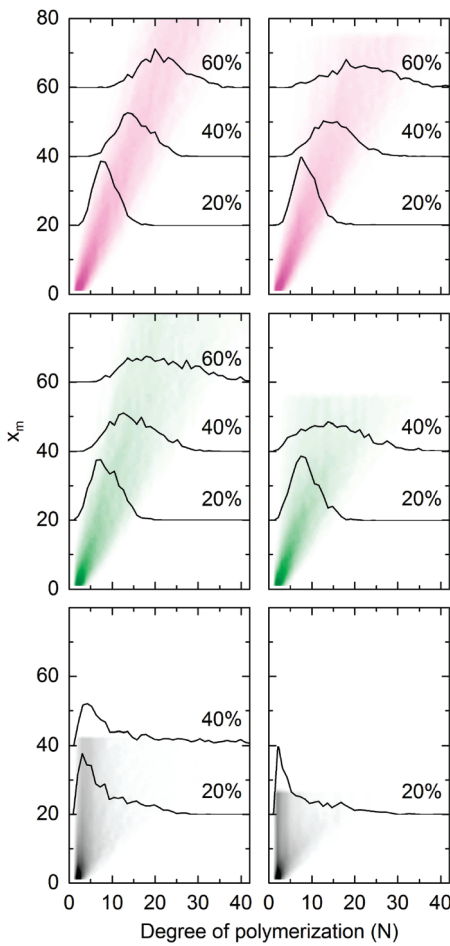


Figure 5. Chain length distributions for surface-initiated polymerizations as a function of monomer conversion (x_m , ordinate) for good (left column, $\epsilon = 4 \times 10^{-7} k_B T$) and poor (right column, $\epsilon = 4 \times 10^{-1} k_B T$) solvent conditions at three grafting densities (σ): 0.08 (top, magenta), 0.16 (middle, green) and 0.44 (bottom, black). The dark areas represent high frequency of a specific chain length and light colors low frequency. The lines represent slices of these distributions and their ordinate value represent the frequency at a given chain length.

commences instantaneously for all growing polymers. In reality, not all initiators are activated at the same time (or activated at all).¹⁹ There are multiple reasons for this behavior. Some of them are associated with the chemical nature of the initiator and the environmental trigger that activates it (typical examples include azo-based initiators for free radical polymerizations^{46–48}) or with steric hindrance of the initiator molecules in confined systems. Because the properties, particularly the PDI, of the polymeric tethers depend crucially on the initiator efficacy, it is important to monitor the fraction of active initiators that participate in the reaction. Although such a task is challenging to carry out experimentally, computer simulations can handle monitoring this parameter very easily. In Figure 4 we plot the fraction of initiators that undergo polymerization as a function of monomer conversion (x_m). For nearly all values of σ , complete (i.e., 100%) initiation efficiency is achieved by $x_m = 0.20$. The sole exceptions are systems with very high grafting density where the initiator efficiency plateaus earlier, $\sigma \geq 0.44$ in good solvents and $\sigma \geq 0.25$ in poor solvents. In poor solvent conditions and at the highest σ , the initiator efficiency reaches a plateau value of 0.8, which might have implications for polymerization of real systems if large gradients in monomer concentration develop (i.e., methacrylates in water/alcohol mixtures).^{19,35}

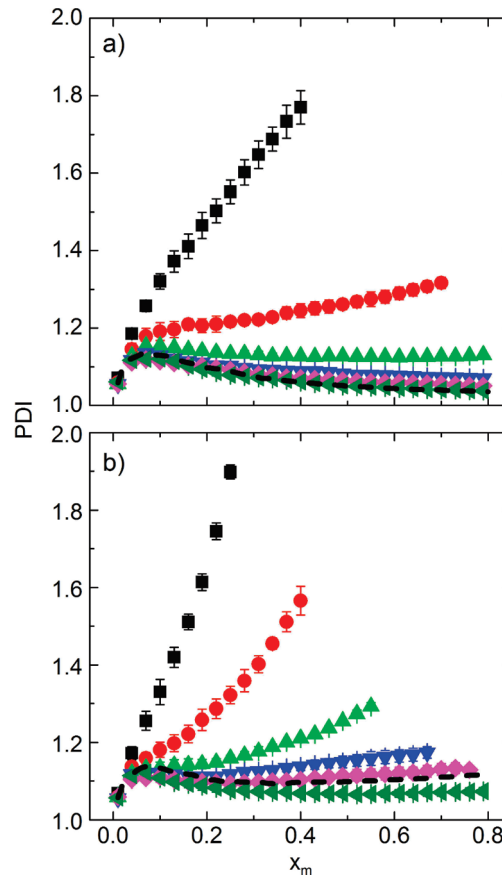


Figure 6. Polydispersity index (PDI) of grafted chains as a function of monomer conversion for good (a, $\epsilon = 4 \times 10^{-7} k_B T$) and poor (b, $\epsilon = 4 \times 10^{-1} k_B T$) solvent conditions at various grafting densities (σ): 0.06 (dark green left-pointing triangle), 0.08 (pink diamond), 0.11 (blue downward triangle), 0.16 (light green triangle), 0.25 (red circle), and 0.44 (black square). The dotted black lines represent the PDI values for chains polymerized in bulk.

One of the main benefits of computer simulations applied to polymerization is that one can determine the MWD of the grown polymers *in situ*. Although SEC experiments are in principle capable of providing similar information, the amount of material cleaved off from the substrate is often below the sensitivity limit of most SEC detectors. Furthermore, even if SEC traces show a polymer peak, they might miss (or skew) low and high molecular weight tails, leading to underestimation of the broadness of the distribution. Computer simulations overcome this limitation by calculating the MWD from the size (N) of each chain. The data in Figure 5 represent MWDs as a function of x_m and σ for good (left column) and poor (right column) solvent conditions. The values in the ordinate represent conversions and the black lines represent slices of the MWDs at the labeled conversions. While relatively narrow peaks represent the MWDs at low σ , at high σ , a high molecular weight tail develops. Going from $\sigma = 0.08$ (top) to $\sigma = 0.44$ (bottom) the MWD broadens significantly. Although at low σ the peak moves steadily to larger molecular weight areas, at high σ , most of the chains remain short. Polymerizations under poor solvents exacerbate these effects, possibly due to chain collapse and obstruction of the access of monomers to chain ends.

To quantify the broadness of the MWDs at different σ and different solvent conditions, we monitor the PDI of the surface-initiated chains as a function of x_m and plot the results in Figure 6. We compute the PDI, defined as the ratio of the mass-average molar mass (second moment) to the

number-average molar mass (first moment) of the distribution, by taking into account the length of all chains including those of initiators that have not yet polymerized ($N = 2$). In good solvents (Figure 6a) and at low σ , the reaction remains controlled; very low PDI values are attainable at all monomer conversions. Furthermore, the PDIs for low σ are identical to those obtained for bulk polymerizations (dashed line). This indicates polymerizations from surfaces populated sparsely with initiators may achieve similar control as the bulk-initiated CRP (we caution that some differences between the two polymerization geometries may still exist in real systems even at low σ because effects not considered in this model, such as mobility of the metal/organic ligand complex, the activation reaction, etc). Increasing σ leads to higher PDI values indicating that polymers grown from dense initiator assemblies have broader MWDs. Given that chain termination is neglected, the monomer concentration is unchanged and all the relevant kinetic parameters of the model are constant, we attribute this gradual increase in PDI to the increase in initiator density on the surface and therefore to chain crowding. This observation is consistent with previous experimental studies^{15,16,18,19} and the work in Liu et al.,³² which report higher PDIs for surface grown polymers relative to polymers grown in solution.

Computer simulations performed under poor solvent conditions yield similar trends as those observed in good solvents. However, we observe pronounced increases in the PDI with increasing monomer conversion, especially at high σ (Figure 6b). At $\sigma = 0.08$, we detect an increase of $\approx 5\%$ in the PDI at the maximum conversion achieved ($x_m = 0.8$) in going from good to poor solvent condition; this value increases to 26% ($x_m = 0.27$) at $\sigma = 0.44$. Overall, there are synergistic effects when both high σ and poor solvent conditions are present that result in very poor control of polymerization reactions. In addition, for the bulk-initiated systems, the increase in PDI when going from good to poor solvent conditions is $\approx 7.8\%$, which is larger than the value at $\sigma = 0.08$. Polymers grown at $\sigma = 0.08$ and under poor solvent conditions represent the only case, in which we observe a lower PDI for grafted chains relative to those in the bulk. A possible explanation for this behavior is that although bulk chains can readily form aggregates through intermolecular interactions, tethered chains cannot diffuse to one another because of their attachment to the surface. The latter prevents chain aggregation and therefore reduces the chain-end confinement on the surface when compared to the bulk.

To explain the increases in PDIs as a function of σ , we recur to the average occupation of the nearest neighbor sites of the active chain-ends. In Figure 7, we plot θ_m , θ_p , and the fraction of surface sites near the chain ends (θ_w) as a function of x_m for polymerizations performed under good (left column) and poor (right column) solvent conditions at three σ values: 0.08 (top), 0.16 (middle), and 0.44 (bottom). We observe that with increasing monomer conversion, θ_m decreases due to monomer consumption, θ_p increases due to the higher molar mass of polymers, and θ_w decreases due to the chain ends moving farther away from the surface. At the lowest σ , the initial value of θ_m ($x_m = 0$) is about half that of the bulk-initiated case and it decreases further at higher values of σ . We attribute this behavior to the presence of the substrate and to the increased crowding of the initiators at higher σ . As the polymerization progresses and the chain ends migrate away from the substrate (at about $x_m = 0.31$), θ_m for the low σ case and the bulk-initiated case become equal, indicating similar environments of the active chain ends in these systems. Further, θ_p increases with increasing σ , indicating that the polymers are occupying the space near the

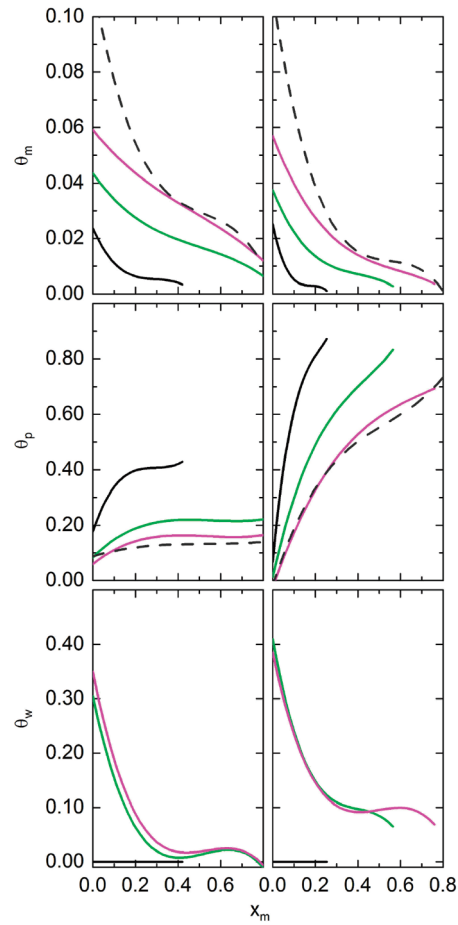


Figure 7. Average number of nearest neighbor sites per active end occupied by monomers (θ_m , top row), polymers (θ_p , middle row), and wall (θ_w , bottom row) as a function of monomer conversion for good (left column, $\epsilon = 4 \times 10^{-7} k_B T$) and poor (right column, $\epsilon = 4 \times 10^{-1} k_B T$) solvent conditions. The solid lines represent values corresponding to various grafting densities: 0.08 (magenta), 0.16 (green), and 0.44 (black). The dark gray dashed lines represent the corresponding values for chains polymerized in bulk.

active chain ends and blocking their access to free monomer. Under poor solvent conditions (right column), this effect is more pronounced suggesting that chain collapse leads to additional masking of the active chain ends by the polymer and additional disruption of the chain-ends access to monomer. Finally, θ_w decreases as a function of x_m except for the largest σ in which its value is zero for all x_m . When $\sigma = 0.44$, the initiators almost fully cover the surface and within the BFM it is impossible for macromolecules growing under such conditions to access the sites adjacent to the wall.

To comprehend the increases in PDI as σ increases, we construct volume fraction profiles of the polymers ($\phi_p(z)$, left column), free monomers ($\phi_m(z)$, center column), and chain ends ($\phi_e(z)$, right column) as a function of distance from the substrate (z , abscissa) and x_m (ordinate) for good (Figure 8) and poor (Figure 9) solvents. As stated previously, the data in the top, middle, and bottom rows correspond to σ equal to 0.08, 0.16, and 0.44, respectively. The colored areas correspond to high concentrations, while the white color denotes zero concentration. The black lines represent sample slices of the $\phi_i(z)$ at a specific x_m . In general, $\phi_p(z)$ and $\phi_e(z)$ extend away from the surface with increasing x_m , as expected. In addition, $\phi_m(z)$ develops a depletion layer near the substrate as x_m increases, indicating that within the polymer brush the concentration of monomer decreases appreciably.

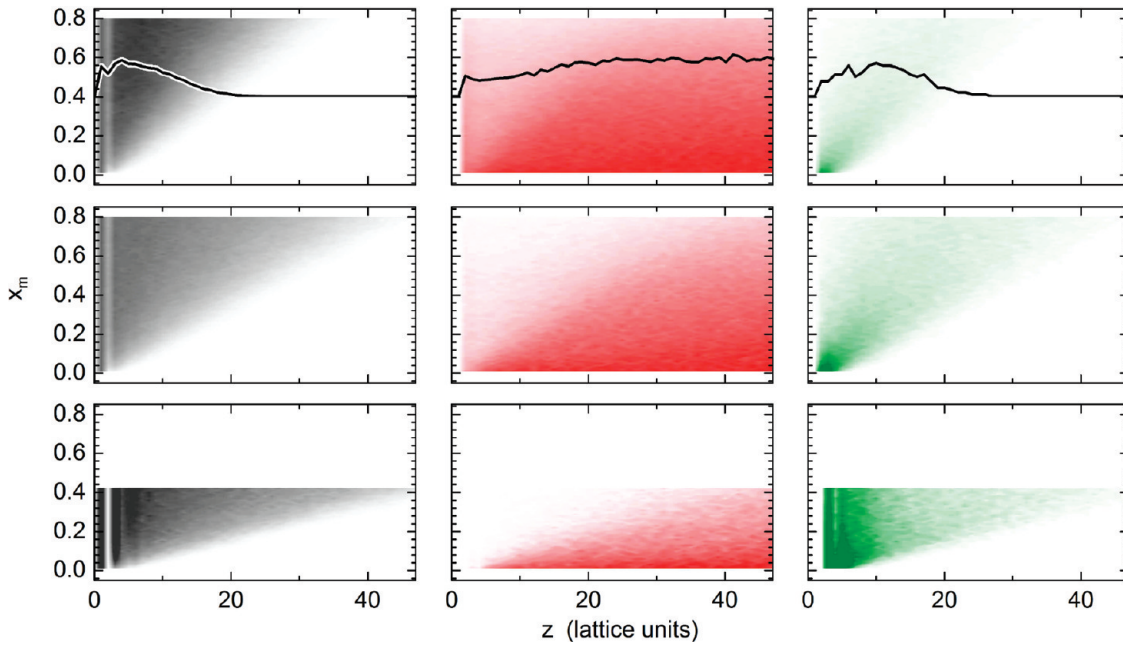


Figure 8. Volume fraction of grafted chains (left column, black), monomers (middle column, red), and chain ends (right column, green) expressed as a function of the distance from the wall (abscissa, z) vs monomer conversion (ordinate, x_m) under good ($\epsilon = 4 \times 10^{-7} k_B T$) solvent conditions at three grafting densities: 0.08 (top row), 0.16 (middle row), and 0.44 (bottom row).

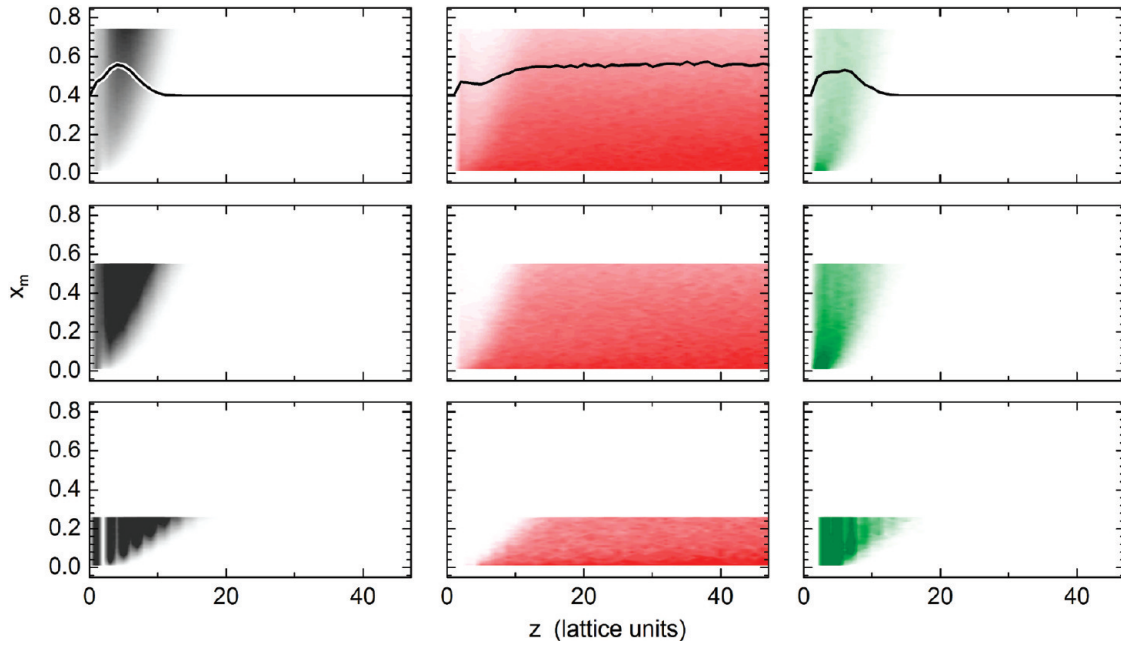


Figure 9. Volume fraction of grafted chains (left column, black), monomers (middle column, red) and chain ends (right column, green) expressed as a function of the monomer conversion (x_m) vs the distance from the wall (z) under poor ($\epsilon = 4 \times 10^{-1} k_B T$) solvent conditions at three grafting densities: 0.08 (top row), 0.16 (middle row), and 0.44 (bottom row).

As σ increases, the monomer depletion continues to develop and reaches a point where the populations of chain ends and monomers no longer overlap. In more detail, Figure 10 shows $\phi_p(z)$, $\phi_m(z)$, and $\phi_e(z)$ on the same scale at three different σ , $x_m = 0.2$ and at good (left column) and poor (right column) solvent conditions. At $\sigma = 0.08$ (top), $\phi_m(z)$ remains almost constant even very close to the surface; there is appreciable overlap between the free monomer and chain-end populations. At $\sigma = 0.16$ (middle), $\phi_m(z)$ undergoes a steeper decrease near the substrate and in poor solvents it is very close to zero. Finally, at $\sigma = 0.44$ (bottom), $\phi_m(z)$ reaches zero farther away from the substrate under both

good and poor solvent conditions. The populations of chain ends and free monomers have minimal overlap leading to uneven growth in the high σ case. We therefore conclude that at higher σ any differences in the chain lengths of the polymers lead to preferential growth of the longer chains versus the shorter ones, a situation that is detrimental to the controlled growth of macromolecules from surfaces.

As alluded to above, properties such as the brush height and the volume fraction profile of the polymers and chain ends depend on the broadness of the MWDs. A brief exploration of these differences can be seen in Figure 11, which shows $\phi_p(z)$ for grafted layers created by our reactive

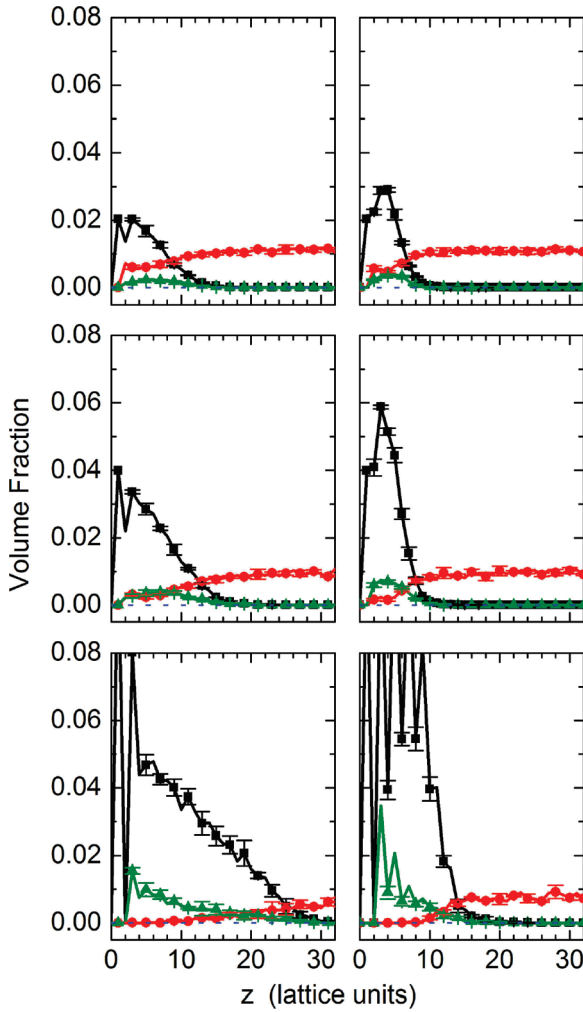


Figure 10. Volume fraction profiles of grafted chains (black square), monomers (red circle), and chain ends (green triangle) for good (left column, $\epsilon = 4 \times 10^{-7} k_B T$) and poor (right column, $\epsilon = 4 \times 10^{-1} k_B T$) solvent conditions at three grafting densities: 0.08 (top row), 0.16 (middle row), and 0.44 (bottom row).

simulation (up-triangles) and those with PDI = 1 (squares). Samples with $N = 10.0$ (10.1 for polydisperse system) correspond to $x_m = 0.26$ and for $N = 20.0$ (20.1 for polydisperse system) correspond to $x_m = 0.58$. As σ increases from 0.11 (top) to 0.25 (bottom), the PDI of the synthesized layers grows from 1.10 to 1.22, respectively, at $N = 10$. Although at $\sigma = 0.11$ the monodisperse and polydisperse concentration profiles are nearly identical, there are substantial differences at $\sigma = 0.25$. Relative to the monodisperse layers, the polydisperse ones exhibit lower $\phi_p(z)$, close to the substrate, but extend farther away from it, indicating larger thicknesses. In general, this effect is more notable as the PDI increases and can be observed for the chains in poor solvents as well.

de Vos and Leermakers recently published a detailed account of the effect of chain length polydispersity on characteristics of end-tethered polymers.²⁹ They used a numerical self-consistent field model to calculate concentration profiles of brushes that had bimodal and continuous distributions (the latter was assumed to follow the Schulz-Zimm distribution). The authors reported that, for both distributions studied, increases in PDI of the brushes in good solvents result in changes in the shape of the concentration profiles from parabolic to linear to concave. They also noted that the average height of the brush increased with increasing PDI; for instance, an increase in PDI from 1.0 to 1.1 resulted in a

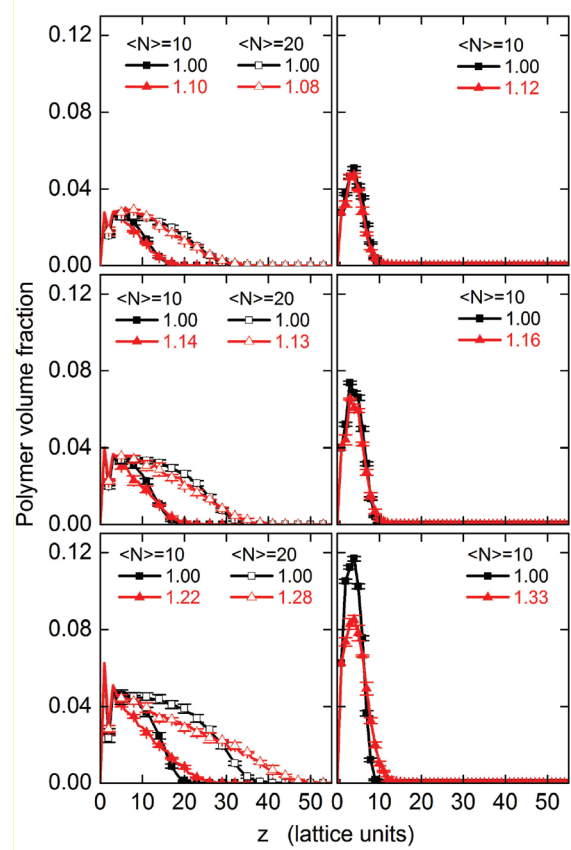


Figure 11. Volume fraction profiles for monodisperse (squares) and polydisperse (triangles, PDI listed in the legend) for good (left column, $\epsilon = 4 \times 10^{-7} k_B T$) and poor (right column, $\epsilon = 4 \times 10^{-1} k_B T$) solvents at three grafting densities: 0.11 (top row), 0.16 (middle row), and 0.25 (bottom row). Profiles were obtained at x_m values of 0.26 and 0.58 for N equal to 10.1 and 20.1, respectively.

12% increase in brush height. de Vos and Leermakers noted that, in polydisperse brushes, chain ends segregate, depending on the molecular weight of the chain as opposed to the monodisperse case, in which the locations of the chain ends fluctuate strongly through the entire thickness of the grafted layer. Our simulations allow us to generate populations of chains grown directly from the surface and determine if the Schulz-Zimm distribution describes correctly these populations. Table 2 shows the least-squared fitted parameters of the Schulz-Zimm distribution to data for several of our grafted polymer populations. Although the Schulz-Zimm distribution describes the populations at $\sigma = 0.08$ and $\sigma = 0.16$ well, at $\sigma = 0.44$ the quality of the fit deteriorates. Moreover, the values obtained for the PDI and N in the high σ fits deviate from the true values for these populations. We posit that the Schulz-Zimm distribution fails to describe the chain-length distribution at high σ because the chains are no longer growing with equal probability, that is, small chains have a lower probability of growth than larger ones. We can also verify independently the conclusions reached by de Vos and Leermakers without assuming any a priori form of the distribution of chain lengths. First, regardless of solvent quality, increasing σ leads to higher PDI and higher brush heights. Second, polydisperse brushes in good solvents are more extended than those in poor solvents, and the latter exhibit larger increases in PDI relative to systems under good solvent conditions. Third, for a given combination of solvent quality, σ , and N , a crossover point exists where all volume fraction profiles intersect regardless of the PDI.

Table 2. Degrees of Polymerization ($\langle N \rangle$) and Polydispersity Indices (PDI) Compared to Those Obtained by Fitting the Schulz-Zimm Distribution to the Simulation Data at Several σ and Both Solvent Conditions

solvent conditions	σ	direct calculation		fit to Schulz-Zimm distribution		
		$\langle N \rangle$	PDI	$\langle N \rangle$	PDI	R^2
good ^a	0.08	14.5	1.07	15.1	1.11	0.96
good ^a	0.16	14.5	1.13	15.2	1.13	0.91
good ^a	0.44	14.5	1.76	10.0	1.76	0.87
poor ^b	0.08	10.4	1.10	10.8	1.09	0.94
poor ^b	0.16	10.4	1.16	11.2	1.16	0.91
poor ^b	0.44	10.4	2.00	3.56	1.62	0.90

^a $\varepsilon = 4 \times 10^{-7} k_B T$, $x_m = 0.40$. ^b $\varepsilon = 4 \times 10^{-1} k_B T$, $x_m = 0.27$.

This observation was also made by de Vos and Leermakers, but not discussed in their paper. We will provide a detailed discussion of this effect in a subsequent publication.⁴⁹

Conclusions

We employed Monte Carlo simulations to investigate the effect that grafting density and solvent quality on surface-initiated living polymerizations. Our computer simulations neglected terminations and chain transfer while incorporating an idealized mechanism for activation and deactivation of the growing chains. We have shown that even under such “true living” conditions “grafting from” polymerization from planar impenetrable substrates results in the broadening of molecular weight distributions relative to bulk-initiated polymerizations and that this broadening increases as the grafting density of initiators increases. We attribute this broadening at high grafting densities to the uneven access of free monomers for short and long chains due to the depletion of free monomer close to substrate. In addition, the PDI of both bulk- and surface-initiated polymers produced by CRP increased with decreasing solvent quality. This behavior has been attributed to the collapsed conformation of the coil and possible chain aggregates that confine the growing chain end and limit the access of free monomers to the growing end. The combination of poor solvent conditions and high grafting densities further exacerbates the broadening of the molecular weight distribution. For instance, relative to good solvent conditions, low grafting density systems ($\sigma = 0.08$) underwent an increase in PDI of 5% under poor solvent conditions. This number increased to 26% at the highest grafting density ($\sigma = 0.44$) studied. We also showed that, although the Schulz-Zimm distribution describes correctly the chain-length probability density of surface-initiated polymers at small and moderate grafting densities, at high grafting densities ($\sigma = 0.44$), the description is no longer valid. We attribute the latter behavior to the difference in the probability of short (low) and long (high) chains to grow, which is a direct result of the separation of the monomer and chain-end populations under these conditions.

Although the effect of initiator density and solvent quality on surface-initiated CRP is clear, additional work is needed to understand the process of living polymerization from surfaces in detail and perhaps in a more realistic manner. One important aspect we have ignored in this work is that solvent quality will depend on the monomer concentration. The interaction energies used in this study could in principle be a function of the distance away from the substrate and depend on the local monomer concentration. This adjustment would resemble experimental conditions more closely. Experimentally, one works with large excess of monomer and stops the reaction in its early stages to keep the PDI relatively low. Computer simulations describing such situations should be developed; this would effectively mean switching from the NVT simulation system to one that considers a constant chemical potential of free monomers in the bulk. A more thorough study is necessary to explore the validity of the Schulz-Zimm distribution for layers polymerized to higher

average degree of polymerization and to check for a crossover degree of polymerization at which the Schulz-Zimm distribution ceases to be valid. The effect of the substrate curvature on the molecular weight (MW) and PDI should also be extended beyond flat surfaces and compared to similar systems polymerized in bulk. In particular, it would be interesting to explore whether strong confinement of chains polymerized from surfaces with negative curvature (i.e., concave surfaces) leads to increases in PDI and decreases in MW. Living polymerization from surfaces with positive curvature (i.e., convex) should also be considered. Here the effect expected is the opposite to polymerization in concave spaces. Specifically, with increasing the positive curvature, the polymers grown from the surface should start to resemble their counterparts polymerized in solution. While the effect of confinement is, in general, relatively trivial to imagine, it is difficult to provide numerical data about the combined effect of curvature, initiator density, and solvent quality. This is where computer simulations will come in very handy.

Acknowledgment. Acknowledgment is made to the Donors of the American Chemical Society Petroleum Research Fund for support of this research under Grant No. 45688-AC7. Partial support from the National Science Foundation through the Grant No. DMR-0906572 is also acknowledged.

Supporting Information Available: The mapping of the coil-to-globule transition and the investigation of the probability of reaction versus motion is presented. This material is available free of charge via the Internet at <http://pubs.acs.org>.

References and Notes

- Barbey, R.; Lavanant, L.; Paripovic, D.; Schüwer, N.; Sugnaux, C.; Tugulu, S.; Klok, H. *Chem. Rev.* **2009**, *109*, 5437–5527.
- Chen, T.; Chang, D. P.; Zauscher, S. *Small* **2010**, *6*, 1504–1508.
- Gautrot, J. E.; Trappmann, B.; Oceguera-Yanez, F.; Connelly, J.; He, X.; Watt, F. M.; Huck, W. T. S. *Biomaterials* **2010**, *31*, 5030–5041.
- Lavanant, L.; Pullin, B.; Hubbell, J. A.; Klok, H. *Macromol. Biosci.* **2010**, *10*, 101–108.
- Moglianetti, M.; Webster, J. R. P.; Edmondson, S.; Armes, S. P.; Titmuss, S. *Langmuir* **2010**, *26*, 12684–12689.
- Ohno, K.; Kayama, Y.; Ladmiral, V.; Fukuda, T.; Tsujii, Y. *Macromolecules* **2010**, *43*, 5569–5574.
- Riachi, C.; Schuwer, N.; Klok, H. *Macromolecules* **2009**, *42*, 8076–8081.
- Takahashi, H.; Nakayama, M.; Yamato, M.; Okano, T. *Biomacromolecules* **2010**, *11*, 1991–1999.
- Ye, Q.; Wang, X.; Li, S.; Zhou, F. *Macromolecules* **2010**, *43*, 5554–5560.
- Tsujii, Y.; Ohno, K.; Yamamoto, S.; Goto, A. Surface-Initiated Polymerization I. In *Advances in Polymer Science*; Jordan, R., Ed.; Springer-Verlag: Berlin/Heidelberg, 2006; Vol. 197, pp 1–45.
- Goto, A.; Fukuda, T. *Prog. Polym. Sci.* **2004**, *29*, 329–385.
- Braunecker, W. A.; Matyjaszewski, K. *Prog. Polym. Sci.* **2007**, *32*, 93–146.
- Matyjaszewski, K.; Miller, P. J.; Shukla, N.; Immaraporn, B.; Gelman, A.; Luokala, B. B.; Siclovan, T. M.; Kickelbick, G.; Vallant, T.; Hoffmann, H.; Pakula, T. *Macromolecules* **1999**, *32*, 8716–8724.

- (14) Matyjaszewski, K.; Dong, H.; Jakubowski, W.; Pietrasik, J.; Kusumo, A. *Langmuir* **2007**, *23*, 4528–4531.
- (15) Gorman, C. B.; Petrie, R. J.; Genzer, J. *Macromolecules* **2008**, *41*, 4856–4865.
- (16) Pasetto, P.; Blas, H.; Audouin, F.; Boissière, C.; Sanchez, C.; Save, M.; Charleux, B. *Macromolecules* **2009**, *42*, 5983–5995.
- (17) Kruk, M.; Dufour, B.; Celer, E. B.; Kowalewski, T.; Jaroniec, M.; Matyjaszewski, K. *Macromolecules* **2008**, *41*, 8584–8591.
- (18) Koylu, D.; Carter, K. R. *Macromolecules* **2009**, *42*, 8655–8660.
- (19) Jones, D. M.; Brown, A. A.; Huck, W. T. S. *Langmuir* **2002**, *18*, 1265–1269.
- (20) Milner, S. T. *Europhys. Lett.* **1988**, *7*, 695–699.
- (21) Milner, S. T.; Witten, T. A.; Cates, M. E. *Macromolecules* **1989**, *22*, 853–861.
- (22) Chakrabarti, A.; Toral, R. *Macromolecules* **1990**, *23*, 2016–2021.
- (23) Klushin, L. I.; Skvortsov, A. M. *Macromolecules* **1992**, *25*, 3443–3448.
- (24) Lai, P.; Zhulina, E. B. *Macromolecules* **1992**, *25*, 5201–5207.
- (25) Dhoot, S.; Watanabe, H.; Tirrell, M. *Colloids Surf., A* **1994**, *86*, 47–60.
- (26) Laub, C. F.; Koberstein, J. T. *Macromolecules* **1994**, *27*, 5016–5023.
- (27) Kritikos, G.; Terzis, A. F. *Polymer* **2005**, *46*, 8355–8365.
- (28) Kritikos, G.; Terzis, A. F. *Polymer* **2007**, *48*, 638–651.
- (29) de Vos, W. M.; Leermakers, F. A. M. *Polymer* **2009**, *50*, 305–316.
- (30) de Vos, W. M.; Leermakers, F. A. M.; de Keizer, A.; Kleijn, J. M.; Cohen Stuart, M. A. *Macromolecules* **2009**, *42*, 5881–5891.
- (31) Wittmer, J. P.; Cates, M. E.; Johner, A.; Turner, M. S. *Europhys. Lett.* **1996**, *33*, 397–402.
- (32) Milchev, A.; Wittmer, J. P.; Landau, D. P. *J. Chem. Phys.* **2000**, *112*, 1606–1615.
- (33) Liu, H.; Li, M.; Lu, Z.; Zhang, Z.; Sun, C. *Macromolecules* **2009**, *42*, 2863–2872.
- (34) Genzer, J. *Macromolecules* **2006**, *39*, 7157–7169.
- (35) Jones, D. M.; Huck, W. T. S. *Adv. Mater.* **2001**, *13*, 1256–1259.
- (36) Schild, H. G.; Muthukumar, M.; Tirrell, D. A. *Macromolecules* **1991**, *24*, 948–952.
- (37) Jones, D. M.; Smith, J. R.; Huck, W. T. S.; Alexander, C. *Adv. Mater.* **2002**, *14*, 1130–1134.
- (38) Farhan, T.; Huck, W. T. S. *Eur. Polym. J.* **2004**, *40*, 1599–1604.
- (39) Liu, G.; Zhang, G. *Langmuir* **2005**, *21*, 2086–2090.
- (40) Jhon, Y. K.; Bhat, R. R.; Jeong, C.; Rojas, O. J.; Szleifer, I.; Genzer, J. *Macromol. Rapid Commun.* **2006**, *27*, 697–701.
- (41) Carmesin, I.; Kremer, K. *Macromolecules* **1988**, *21*, 2819–2823.
- (42) Deutscher, H. P.; Binder, K. *J. Chem. Phys.* **1991**, *94*, 2294–2304.
- (43) Wittkop, M.; Kreitmeier, S.; Göritz, D. *J. Chem. Phys.* **1996**, *104*, 3373–3385.
- (44) Semler, J. J.; Genzer, J. *J. Chem. Phys.* **2006**, *125*, 014902.
- (45) Matyjaszewski, K.; Xia, J. H. *Chem. Rev.* **2001**, *101*, 2921–2990.
- (46) Prucker, O.; Ruhe, J. *Macromolecules* **1998**, *31*, 602–613.
- (47) Prucker, O.; Ruhe, J. *Macromolecules* **1998**, *31*, 592–601.
- (48) Prucker, O.; Ruhe, J. *Langmuir* **1998**, *14*, 6893–6898.
- (49) Turgman-Cohen, S.; Genzer, J. Manuscript in preparation.